X. Q. Shi, W. Zhou, H. L. J. Pang, and Z. P. Wang, Effect of Temperature and Strain Rate on Mechanical Properties of 63Sn/37Pb Solder Alloy, ASME Journal of Electronic Packaging, ASME, USA, Vol. 121, No. 3, 1999, pp. 179-185. You are welcome to e-mail Prof. Wei Zhou at WZhou@Cantab.Net for further inquiries.

Effect of Temperature and Strain Rate on Mechanical Properties of 63Sn/37Pb Solder Alloy

X. Q. Shi, W. Zhou*, H. L. J. Pang*, and Z. P. Wang

Gintic Institute of Manufacturing Technology, Nanyang Drive, Singapore 638075

*School of Mechanical & Production Engineering, Nanyang Technological University, Singapore 639798

In this study, tensile tests of 63Sn/37Pb solder were carried out at various strain rates from 10^{-5} s^{-1} to 10^{-1} s^{-1} over a wide temperature range from – 40 °C to 125 °C to study the effect of strain rate and testing temperature on the mechanical properties in a systematic manner. Based on these experimental data, a set of empirical formulae was derived by a statistical method to describe the effect of temperature and strain rate in a quantitative manner and explain the variation in the mechanical properties published in other reports. It is concluded that the empirical formulae can be used to characterize the mechanical properties of 63Sn/37Pb over a wide range of temperatures and strain rates.

1. Introduction

Solder alloys are commonly used in surface mount technology (SMT) as an interconnect material for electrical connections and also serves as the mechanical support to hold the component in position on the printed circuit board (PCB). Since solder joints are usually subject to thermo-mechanical stresses at the operating temperature as high as 0.5 to 0.8 times T_m (melting temperature) of the alloy, a significant amount of deformation is introduced by plasticity and creep throughout the strain cycle. The thermal and mechanical reliability of surface mounted solder joints is one of the major issues that hinder the development of packages towards small print and high density connections with robust reliability. For reliability analysis of solder joints, it is necessary

and important to understand the mechanical properties of solder alloys. In the past decade, much research has been carried out to study the mechanical properties of solder alloys (Vaynman et al., 1989; Kilinski et al., 1991; Skipor et al. 1996; Liu et al., 1997; Lau et al, 1997). However, the researchers in the area only focus on the effect of temperature, there is only a rare investigation on the effect of strain rate (Ninomiya et al., 1997). And the experimental results obtained by different researchers vary widely depending on the test condition for nominally the same solder alloy type. For example, Young's modulus of 63Sn/37Pb solder can vary from a minimum of 0.9 GPa (Jones et al., 1997) to a maximum of 36 GPa (Lau et al., 1997) for different test temperatures and strains. A comparison on the reported experimental data and test condition for several typical publications will be given and discussed in section 5. It is believed that the apparently large discrepancy among the different studies is mainly due to the differences in the test temperature and strain rate performed in different laboratories. Hence, it is necessary to investigate the effect of temperature and strain rate on the mechanical properties in a systematic manner.

The temperature ramp rates of the accelerated thermal cycling (ATC) tests, carried out at different laboratories, can vary from 8 ^{o}C/min to 20 ^{o}C/min (JEDEC standard, 1989). While the temperature ramp rate can be even as high as 50 ^{o}C/min in a thermal shock test, which is used to assess the package resistance to sudden temperature change (JEDEC standard, 1995). Therefore, it is desirable to study the mechanical properties at a wide range of temperatures and strain rates to interpret the results in these acceleration tests.

In the present study, tensile tests of 63Sn/37Pb solder were carried out at various strain rates from 2.78×10^{-5} s^{-1} to 2.78×10^{-1} s^{-1}, over a wide temperature range from -40 ^{o}C to 125 ^{o}C, to investigate the effect of test temperature and strain rate on the mechanical properties in a systematic manner.

2. Experimental Procedures

The uniaxial tension method was employed to test the mechanical properties of 63Sn/37Pb solder alloy. The chemical composition of this solder studied is as follows (wt.%): 63.2 Sn, remainder Pb, 0.006 Sb, 0.002 Cu, 0.004 Bi, 0.001 Zn, 0.002 Fe, 0.001 Al, 0.01 As, and 0.001 Cd. Dog bone-shaped bulk solder specimens for the uniaxial tensile test were prepared, by machining from the high purity as-cast original 63Sn/37Pb solder bar, in accordance with ASTM standards. The specimens had a total length of 90 mm, a gage length of 30 mm, and a diameter of 6 mm. After machining, the gauge section of each specimen was carefully ground on SiC paper and polished using 1.0 μm diamond paste. The tensile specimens were then annealed for 24 hours at 60 ^{o}C in a N_2 atmosphere to eliminate the surface residual stresses.

Tensile tests were carried out on a universal testing machine, Instron model 4206, at four different temperatures (– 40 ^{o}C, 25 ^{o}C, 75 ^{o}C, and 125 ^{o}C). At each test temperature, five different strain rates were used (2.78×10^{-5} s^{-1}, 2.78×10^{-4} s^{-1}, 2.78×10^{-3} s^{-1}, 2.78×10^{-2} s^{-1}, and 2.78×10^{-1} s^{-1}). Three samples per test condition were used and the results were averaged to reduce the experimental error. In order to perform testing over the range of – 40 ^{o}C to 125 ^{o}C, the tensile tester was fitted with a thermally insulated chamber. A dynamic extensometer was employed in the specimen gauge section to measure the true extension of specimen rather than the crosshead movement. A computer with the data acquisition software was used to collect the data.

After specimen grips and environmental chamber have reached thermal equilibrium, the specimen was placed into the chamber for a minimum of half an hour prior to testing. For high temperature tests (75 ^{o}C and 125 ^{o}C), four pieces of metal foil with a number of holes were made to increase the friction between the grips and a specimen. A rubber band was employed to support the extensometer in order to reduce the contact force on the specimen. In addition, the extensometer's anti-slip blades were blunted to prevent them from damaging the specimen. For low temperature

tests (– 40 ^{o}C), liquid nitrogen was used to obtain the required testing temperature. The specimen temperature was monitored by a thermo-couple. A feed-back control was used to regulate the testing temperature by either directing electric current through heating panels or regulating the flow of liquid nitrogen to the temperature chamber.

3. Experimental Results

By plotting all the stress-strain curves under each isothermal condition into one graph, the effect of strain rate and temperature on the 63Sn/37Pb tensile properties could be evaluated and compared. The typical stress-strain curves at a constant temperature of 25 ^{o}C and a constant strain rate of 2.78×10^{-3} s^{-1} are shown in Figs. 1 and 2, respectively. It is noted that the mechanical properties of 63Sn/37Pb are strongly dependent on the test temperature and strain rate parameters. The effect of these parameters on Young's modulus, yield stress, ultimate tensile strength (UTS), and elongation was investigated individually in the following sections:

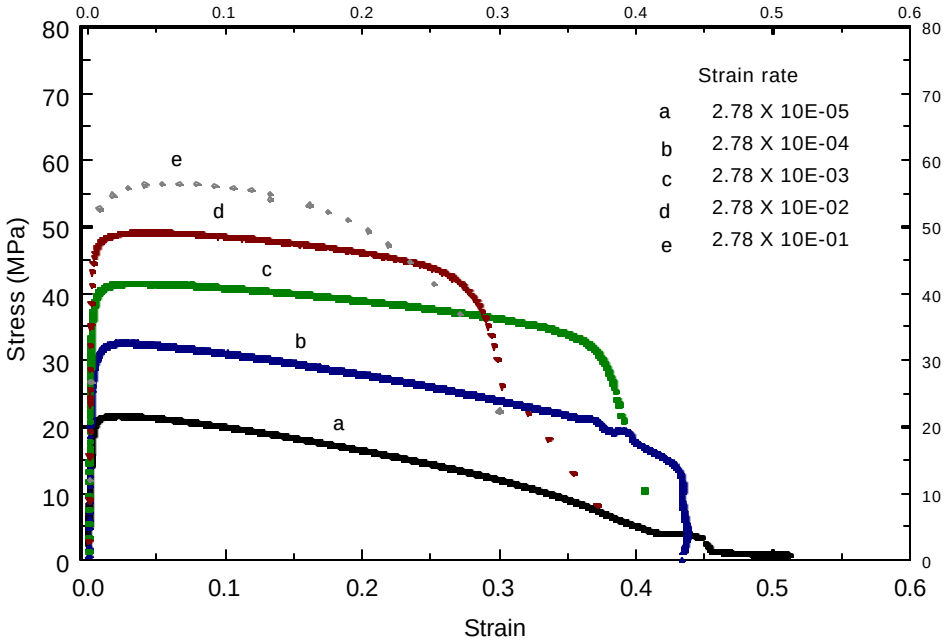

Fig. 1 Typical stress-strain curves at a constant temperature of 25 ^{o}C showing effect of different strain rates

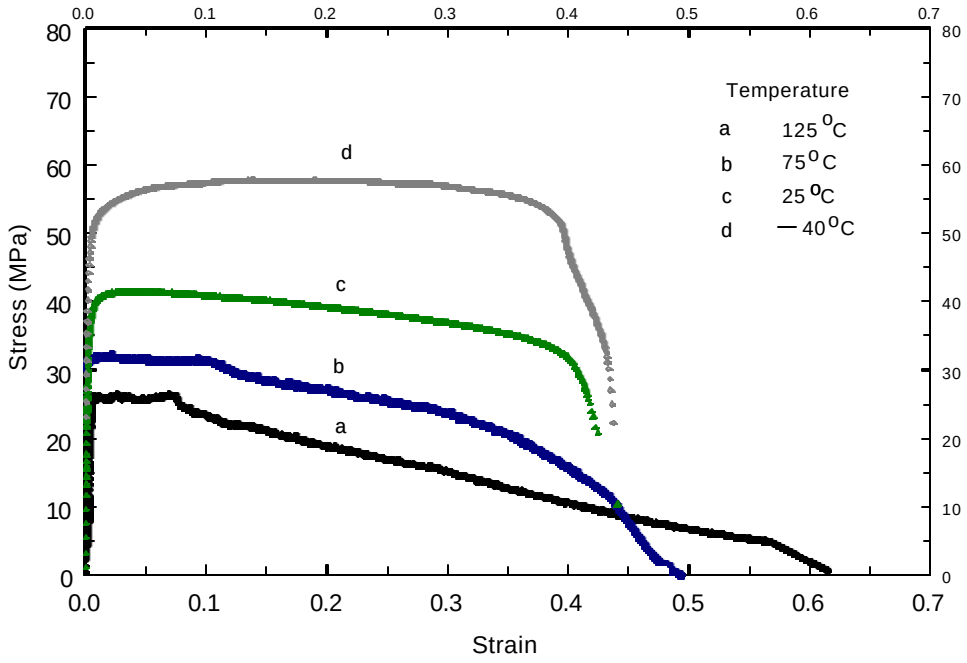

Fig. 2 Typical stress-strain curves at a constant strain rate of 2.78×10^{-3} s^{-1} showing effect of different temperatures

3.1 Effect of temperature and strain rate on Young's modulus

The slope between the origin and a point of the elastic section in the stress-strain curve is taken as the Young's modulus. To eliminate the effect of inelastic deformation and to get the accurate value of the slope, the strain axis in the stress-strain plot is magnified to make the elastic section of the stress-strain curve fall between the slope of 45^o to 60^o. The result of the effect of temperature on Young's modulus is shown in Fig. 3. It can be seen that the curves demonstrate linear relationship between Young's modulus and temperature. The effect of strain rate on Young's modulus is presented by plotting the graph of Young's modulus versus strain rate as shown in Fig. 4. The plot shows approximately straight lines with a constant slope for any given temperature. This is expected as the Young's modulus has a linear function of logarithmic strain rate.

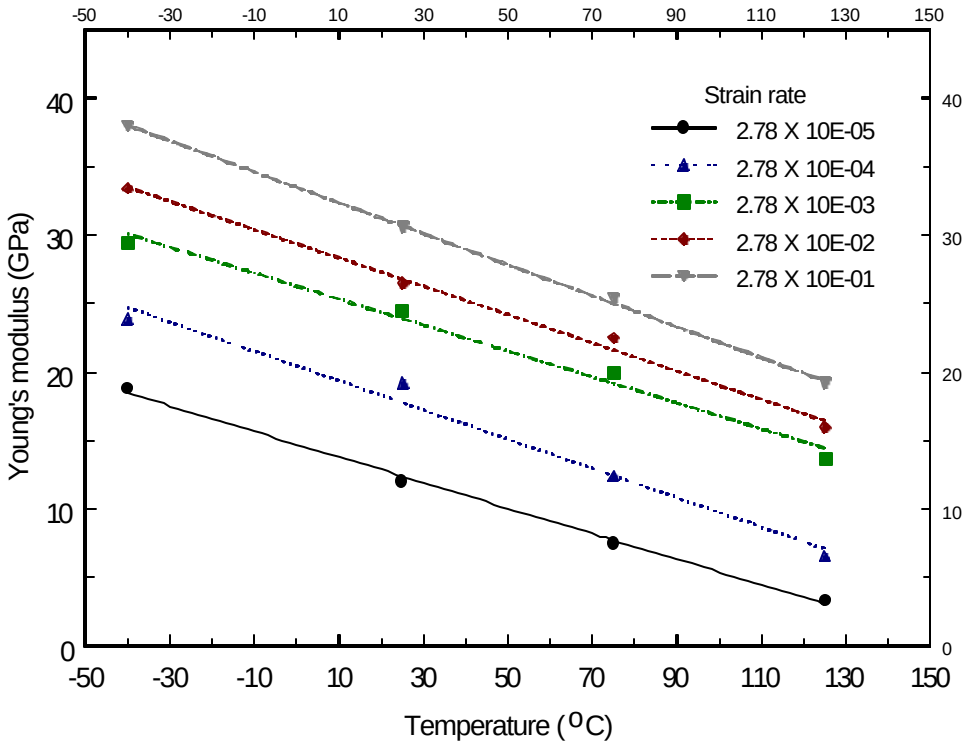

Fig. 3 Effect of temperature on Young's modulus

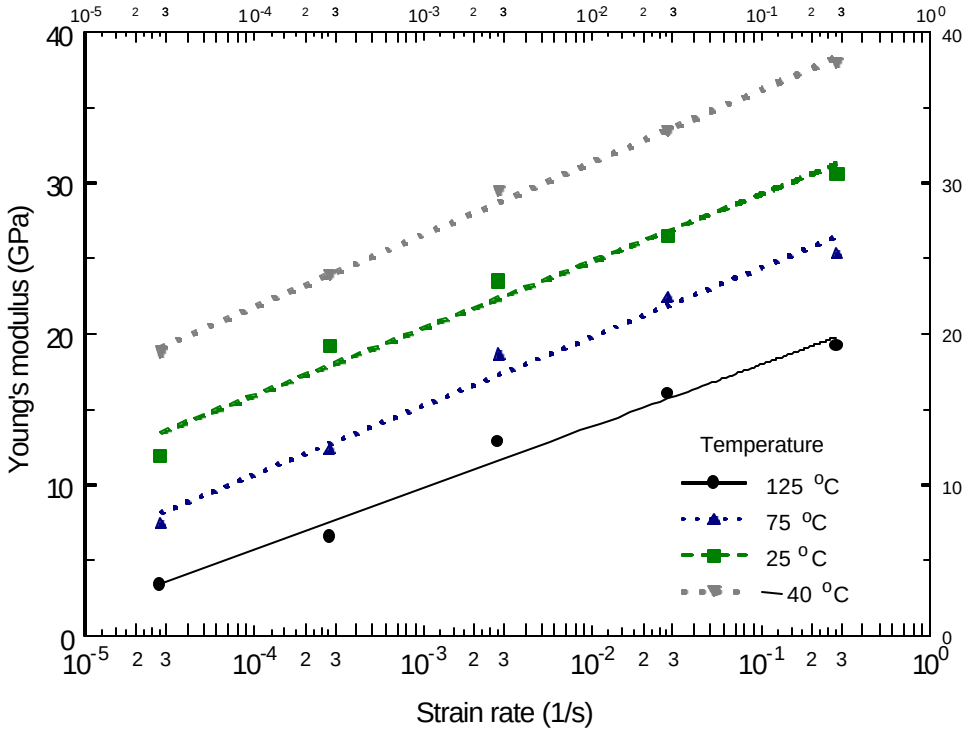

Fig. 4 Effect of strain rate on Young's modulus

3.2 Effect of temperature and strain rate on yield stress

The stress at 0.2% strain in stress-strain curve is taken as yield stress. For the same reason mentioned in section 3.1, the elastic section of stress-strain curve has to be adjusted so that it falls within the slope of 45^{o} to 60^{o}. Fig. 5 presents the effect of temperature on yield stress. As can be seen, there is an approximately linear relationship between the yield stress and temperature. The effect of strain rate on yield stress is plotted in Fig. 6 at different temperatures. It is noted that yield stress increases with strain rate in a non-linear manner. Two trends were noted. Firstly, the slope of each curve is different at each temperature and increases with increasing temperature. The curve at – 40 °C is approximately linear on the log-log plot and becomes increasingly non-linear as the test temperature is increased to 125 °C. Another trend noted is that the variation in yield stress is wider at lower strain rate than that at higher strain rate. This is expected as the creep deformation makes larger contribution to the strength reduction at higher temperature or at lower strain rate. At lower test temperature or higher strain rate, the creep deformation is expected to be smaller.

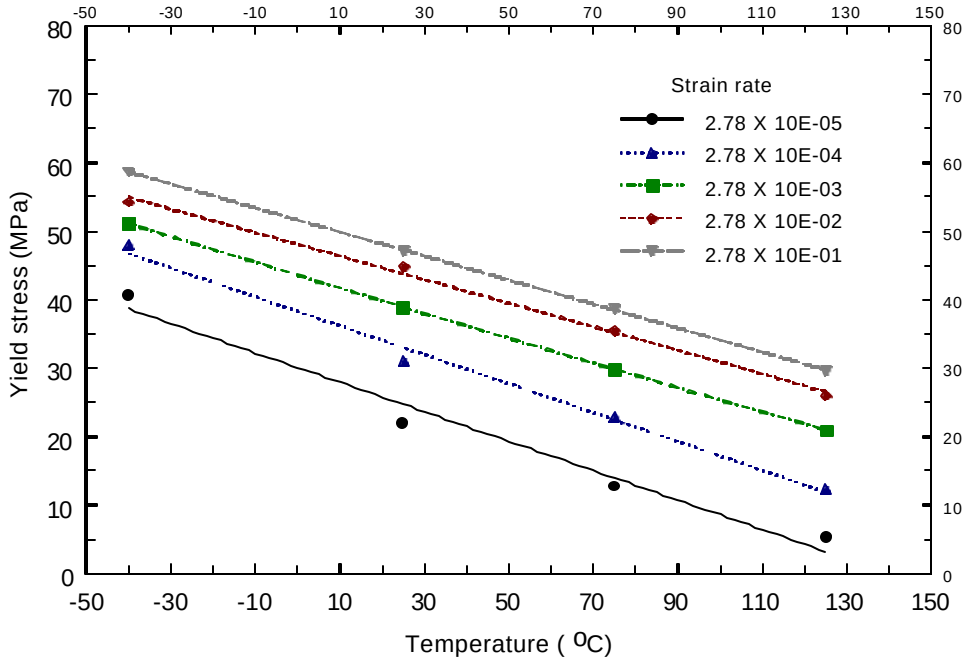

Fig. 5 Effect of temperature on yield stress

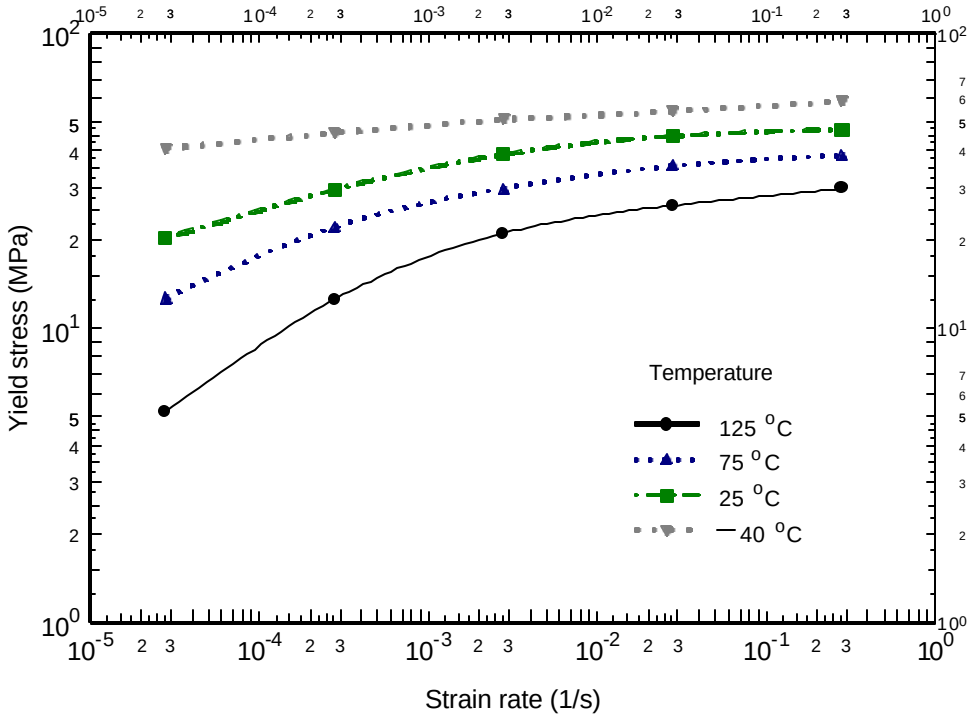

Fig. 6 Effect of strain rate on yield stress

3.3 Effect of temperature and strain rate on UTS

The value corresponding to the maximum stress in the stress-strain curve is taken as ultimate tensile strength (UTS). Fig. 7 shows the UTS decreases with the temperature. From Fig. 8, it can be seen that at lower temperature, UTS has an approximately linear relation with strain rate, while at higher temperature, the UTS becomes increasingly non-linear manner just like the trends for yield stress plotted in Fig. 6.

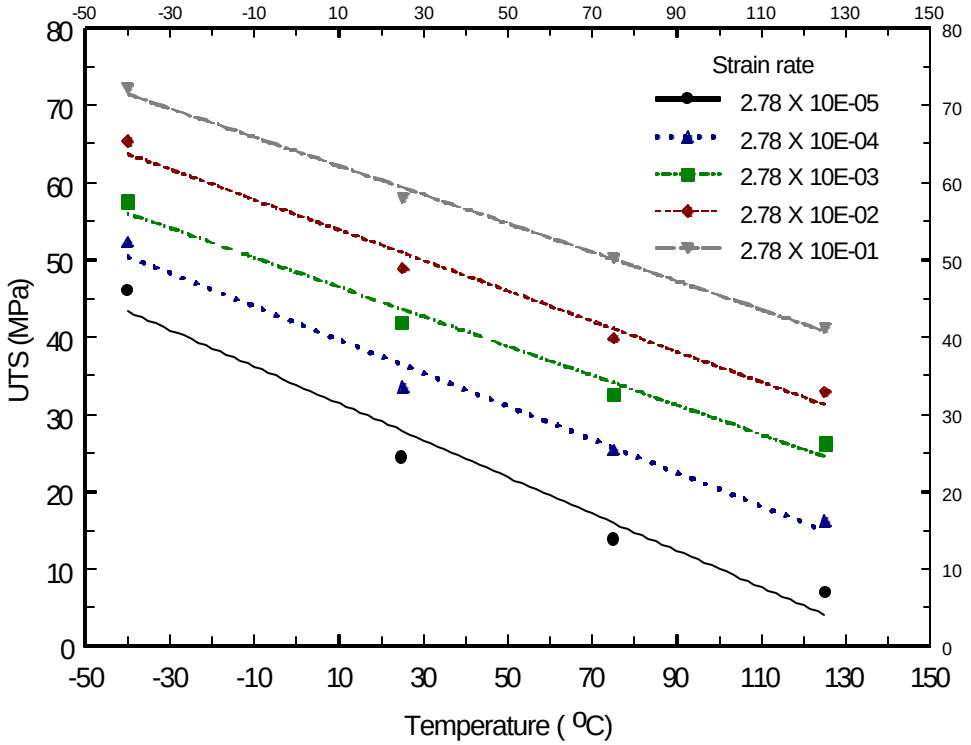

Fig. 7 Effect of temperature on UTS

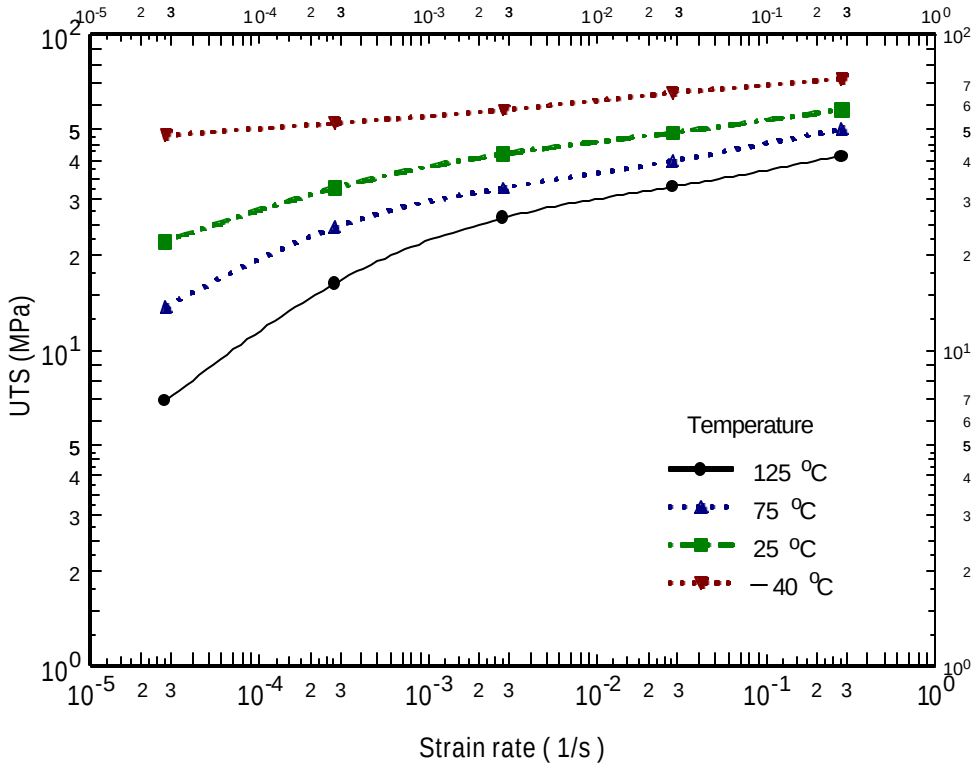

Fig. 8 Effect of strain rate on UTS

3.4 Effect of temperature and strain rate on elongation

The elongation δ was calculated using the following equation:

$$d = \frac{L_f - L_o}{L_o} \qquad (1)$$

where L_o is the original gauge length and L_f is the gauge length at fracture. The elongations are shown in Fig. 9(a) as a function of temperature and strain rate. It can be seen that the elongation increases with decreasing strain rate in the higher temperature range 25 ^{o}C to 125 ^{o}C. However, it is intriguing to observe that the relationship between elongation and strain rate is exactly reversed at – 40 ^{o}C. That is to say, at – 40 ^{o}C elongation increases with increasing strain rate. To examine the "unusual" phenomenon further, additional tensile tests were conducted at – 10 ^{o}C and – 50 ^{o}C using five strain rates (2.78×10^{-1}, 2.78×10^{-2}, 2.78×10^{-3}, 2.78×10^{-4}, and 2.78×10^{-5} s^{-1}), at – 75 ^{o}C using three strain rates (2.78×10^{-1}, 2.78×10^{-2}, and 2.78×10^{-3} s^{-1}), and at – 100 ^{o}C using three strain rates (2.78×10^{-1}, 2.78×10^{-3}, and 2.78×10^{-5} s^{-1}), respectively. The elongations obtained from the additional tests are shown in Fig. 9(b). It is clear from the figure that elongation of the solder reaches a peak value at approximately – 50 ^{o}C for any given strain rate. The peak value of elongation at – 50 ^{o}C is also found to be related to the testing strain rate: it increases with increasing strain rate in the strain rate range of 2.78×10^{-5} s^{-1} to 2.78×10^{-2} s^{-1} and reaches the maximum value at a strain rate of 278×10^{-2} s^{-1}; however, it decreases when the strain rate increases further from 2.78×10^{-2} s^{-1} to 2.78×10^{-1} s^{-1}. This indicates that elongation reaches its maximum value at the optimum deformation temperature of – 50 ^{o}C and strain rate 2.78×10^{-2} s^{-1}.

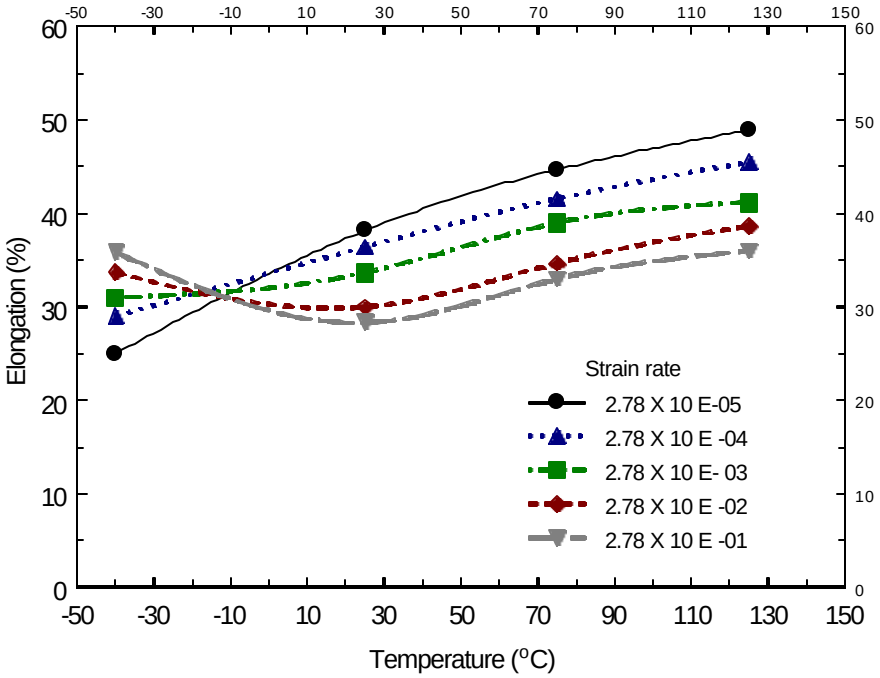

(a)

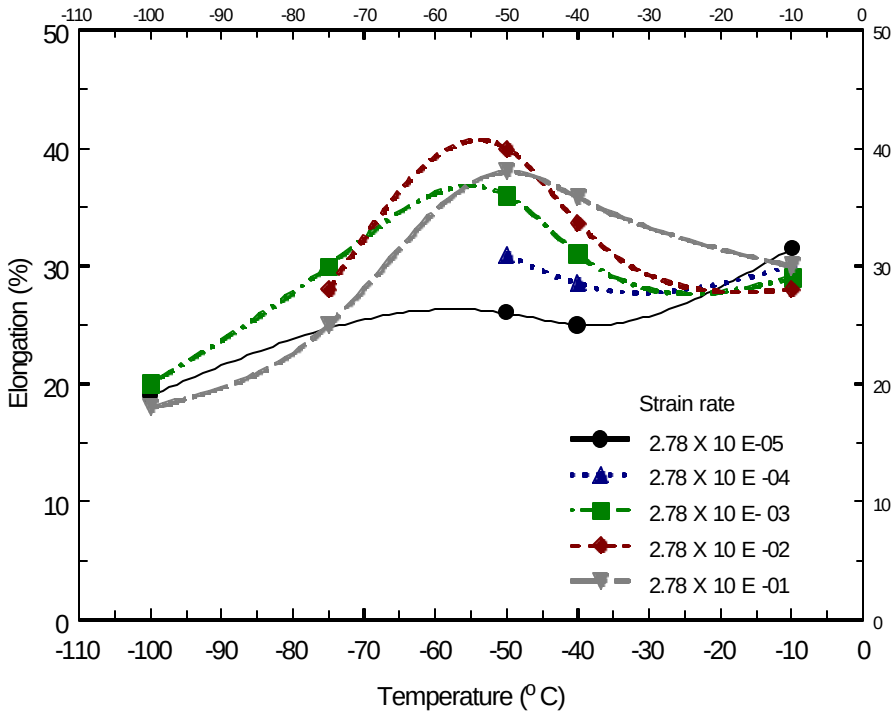

(b)

Fig.9 Effect of temperature and strain rate on elongation at different temperature ranges: (a) – 40 °C ~ 125 °C, (b) – 100 °C ~ – 10 °C

The above observation might seem to be "unexpected", but in fact it is typical behaviour for materials displaying superplasticity (Kondo et al., 1997, Li et al., 1997, Han et al., 1997, Furukawa et al., 1998). At high temperatures, elongation of materials does not always increase with increasing temperature or decreasing strain rate, and the best ductility is usually obtained at a certain temperature and strain rate, as observed in the present study. A possible explanation to this phenomenon is that the peak value of elongation at high temperature results from the interaction between work hardening and dynamic recovering.

The solder has a melting point (T_m) of 183 ^oC (456 K), so it should be noted that test temperature – 50 ^oC (223 K) corresponds to about $0.5T_m$ (in K) and therefore should be regarded as a high temperature for this particular material. At temperatures lower than – 50 ^oC (*i.e.*, lower than $0.5\ T_m$), the plastic deformation is dominated by the dislocation movement within the grains. When the solder is deformed, necking occurs with increasing plastic strain, and the work hardening around the neck results in increasing resistance to deformation. When the deformation resistance reaches the critical value, the material fractures. However, when the deformation temperature increases to around T_c = – 50 ^oC ($0.5\ T_m$), the dynamic recrystallization recovering energy Q_{rec} is so high that the solder material is activated and dynamic recrystallization can occur during testing. The recrystallization changes the deformed grains into dislocation-free fine grains and thus reduces the strain hardening in the neck. This process makes it easier for the neck to diffuse, leading to larger elongation. However, when the temperature is in the range just above T_c, the strength of grain decreases, making the diffusion of neck difficult and resulting in lower elongation.

The process of dynamic recrystallization at temperatures close to T_c is also affected by strain rate (see Fig. 10). On the one hand, if the strain rate is too low, the testing time is very long, and therefore the grains will have sufficient time to grow coarse after full recrystallization (Fig. 10(b)), leading to lower elongation. On the other hand, if the strain rate is too high, the recrystallization is

negligible or incomplete during the short testing period, and this also results in relatively low elongation. According to this analysis, the largest elongation can only be obtained when the strain rate is optimum so that the testing time is long enough for dynamic recrystallization to occur but short enough to avoid excessive grain growth.

.

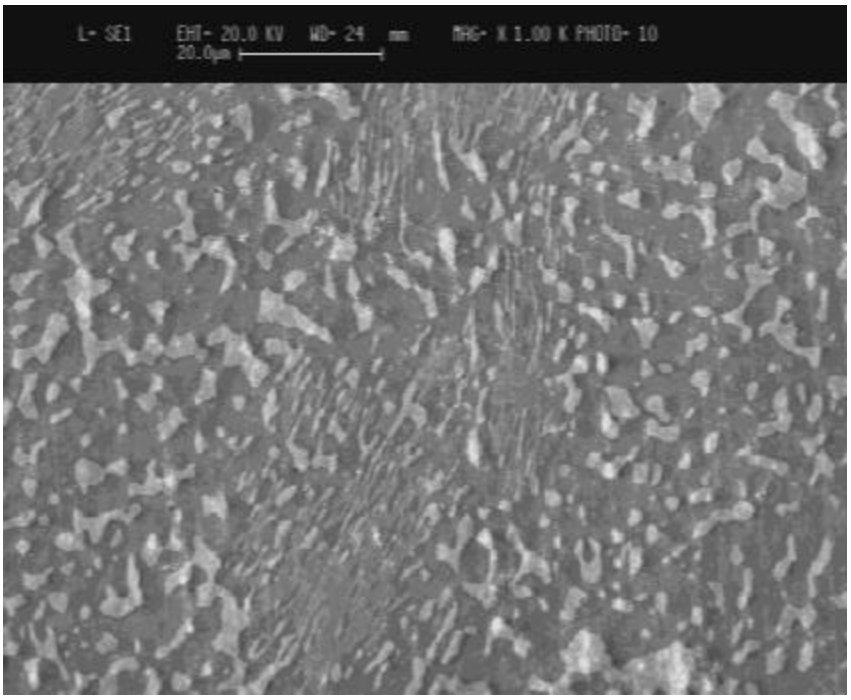

(a)

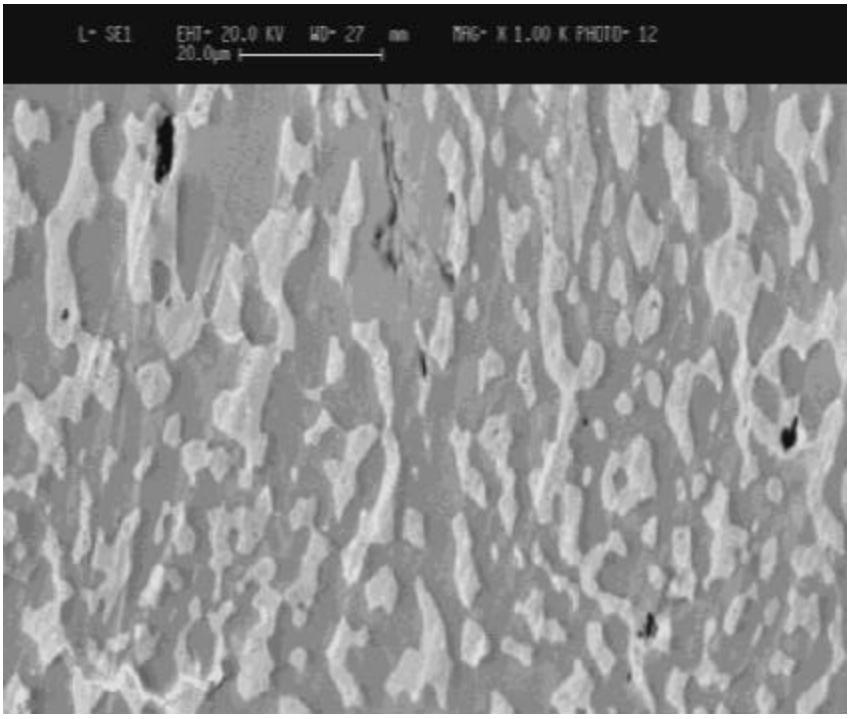

(b)

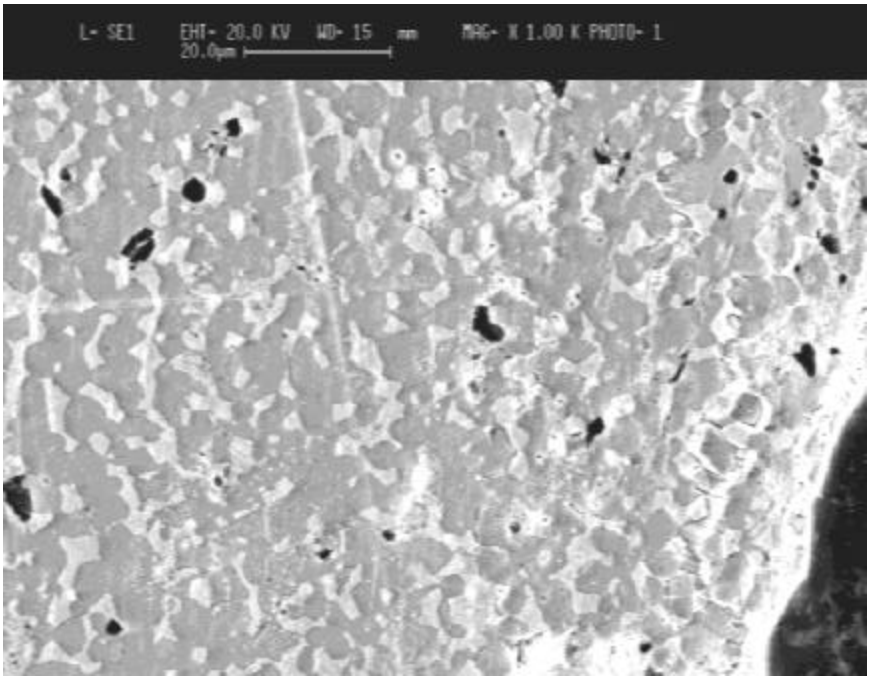

(c)

Fig.10 Microstructure evolution at -40 ^{o}C for different strain rates: (a) original microstructure (before testing); (b) coarse microstructure after being tested at the lowest strain rate of 2.78×10^{-5}; (c) microstructure after being tested at the highest strain rate of 2.78×10^{-1}.

4. Derivation of Empirical Formulae

In most reported solder properties, only the temperature dependent mechanical properties of solder alloys have been presented as linear equations with respect to temperature (Lau et al., 1997). It is not adequate just to use existing temperature dependent mechanical properties to understand the failure of solder joints and the reliability of surface mount assemblies. The solder properties are dependent both on temperature and strain rate, and it would be very useful to curve-fit the wide range of test result to a single equation that is temperature and strain rate dependent. So using our experimental data, a statistical method incorporating multiple linear regression was employed to identify the temperature and strain rate dependent mechanical properties of 63Sn/37Pb solder.

4.1 Young's modulus

Assuming that the constitutive model for Young's modulus can be written as:

$$E(T,\dot{e}) = (a_3 T + a_2)\log(\dot{e}) + (a_1 T + a_0) + d \qquad (2)$$

where $\dot{e}$ is the strain rate; T is the temperature; a_0, a_1, a_2, and a_3 are unknown constants; δ is the error term which is introduced to account for any experimental error. For constant temperature, introducing two temperature dependent constants $a(T) = a_3 T + a_2$ and $b(T) = a_1 T + a_0$, equation (2) can be simplified as

$$E = a(T)\log(\dot{e}) + b(T) + d \qquad (3)$$

Based on the linear equation (3), a linear estimator equation can be formulated

$$\hat{E} = \hat{a}\log(\dot{e}) + \hat{b} \qquad (4)$$

where $\hat{E}, \hat{a}, \hat{b}$ are estimated values of E, α, and β, respectively. It is now necessary to rewrite

equation (4) in matrix notation in the form

$$Y = X \times C \tag{5}$$

to apply multiple linear regression with

$$Y = \begin{bmatrix} E_1 \\ E_2 \\ \vdots \\ E_{15} \end{bmatrix} \quad X = \begin{bmatrix} \log(\dot{e}_1) & 1 \\ \log(\dot{e}_2) & 1 \\ \vdots & \vdots \\ \log(\dot{e}_{15}) & 1 \end{bmatrix} \quad C = \begin{bmatrix} a \\ b \end{bmatrix} \tag{6}$$

For each given testing temperature (– 40 ^{o}C, 25 ^{o}C, 75 ^{o}C, and 125 ^{o}C), tests were repeated three times at the same strain rates of 2.78×10^{-5} s^{-1}, 2.78×10^{-4} s^{-1}, 2.78×10^{-3} s^{-1}, 2.78×10^{-2} s^{-1}, 2.78×10^{-1} s^{-1}. Using these experimental data, the temperature dependent constants can be derived from calculus, where the estimated coefficient matrix, $\hat{C}$, is found from the solution to the equation:

$$\hat{C} = \left(X^T X\right)^{-1} X^T Y \tag{7}$$

where $\hat{C} = \begin{bmatrix} \hat{a} \\ \hat{b} \end{bmatrix}$. However, the temperature dependent constants α, β also can be expressed by the matrix notation forms

$$\begin{cases} Y_1 = X_1 \times C_1 \\ Y_2 = X_2 \times C_2 \end{cases} \tag{8}$$

where

$$Y_1 = \begin{bmatrix} a_1 \\ a_2 \\ a_3 \\ a_4 \end{bmatrix} \quad X_1 = \begin{bmatrix} T_1 & 1 \\ T_2 & 1 \\ T_3 & 1 \\ T_4 & 1 \end{bmatrix} \quad C_1 = \begin{bmatrix} a_3 \\ a_2 \end{bmatrix} \quad Y_2 = \begin{bmatrix} b_1 \\ b_2 \\ b_3 \\ b_4 \end{bmatrix} \quad X_2 = \begin{bmatrix} T_1 & 1 \\ T_2 & 1 \\ T_3 & 1 \\ T_4 & 1 \end{bmatrix} \quad C_2 = \begin{bmatrix} a_1 \\ a_0 \end{bmatrix}$$

Thus, the constants a_0, a_1, a_2, and a_3 can be determined from calculus that the estimated coefficient matrix, $\hat{C}_1, \hat{C}_2$, are calculated as:

$$\hat{C}_1 = \left(X_1^T X_1\right)^{-1} X_1^T Y_1 \tag{9}$$

$$\hat{C}_2 = \left(X_2^T X_2\right)^{-1} X_2^T Y_2 \tag{10}$$

where

$$\hat{C}_1 = \begin{bmatrix} \hat{a}_3 \\ \hat{a}_2 \end{bmatrix}, \quad \hat{C}_2 = \begin{bmatrix} \hat{a}_1 \\ \hat{a}_0 \end{bmatrix}$$

By solving equations (7), (9), and (10), and substituting the solutions of constants of a_0, a_1, a_2, and a_3 into equation (2), the constitutive model of Young's modulus is finally obtained:

$$E(T,\dot{e}) = (-0.006T + 4.72)\log(\dot{e}) + (-0.117T + 37) \tag{11}$$

4.2 Yield stress and ultimate tensile strength

Based on the experimental results, it can be assumed that both yield stress and UTS are related to the temperature and strain rate by the linear function and logarithmic function, respectively. To fit the experimental data, bi-linear constitutive models for yield stress and UTS were established and expressed individually as follows:

$$\sigma_y(T,\dot{e}) = \begin{cases} a_1(T)(\dot{e})^{b_1(T)} & for \quad \dot{e} \geq 5\times10^{-4} \\ a_2(T)(\dot{e})^{b_2(T)} & for \quad \dot{e} < 5\times10^{-4} \end{cases} \tag{12}$$

where $\dot{e}$ is the strain rate, T is the temperature, and

$$\begin{cases} a_1(T) = b_1 T + b_0 \\ a_2(T) = b_1' T + b_0' \\ b_1(T) = b_3 T + b_2 \\ b_2(T) = b_3' T + b_2' \end{cases}$$

here $b_0, b_0', b_1, b_1', b_2, b_2', b_3, b_3'$ are unknown constants.

$$\sigma_{UTS}(T,\dot{\varepsilon}) = \begin{cases} a_1(T)(\dot{\varepsilon})^{b_1(T)} & for \quad \dot{\varepsilon} \geq 5\times 10^{-4} \\ a_2(T)(\dot{\varepsilon})^{b_2(T)} & for \quad \dot{\varepsilon} < 5\times 10^{-4} \end{cases} \tag{13}$$

where $\dot{\varepsilon}$ is the strain rate, T is the temperature, and

$$\begin{cases} a_1(T) = c_1 T + c_0 \\ a_2(T) = c_1' T + c_0' \\ b_1(T) = c_3 T + c_2 \\ b_2(T) = c_3' T + c_2' \end{cases}$$

here $c_0, c_0', c_1, c_1', c_2, c_2', c_3, c_3'$ are unknown constants. Follow the same evolution procedure to establish the constitutive model of Young's modulus, the constants of constitutive models for yield stress and UTS can be determined. Finally, the constitutive models of yield stress and UTS are obtained individually:

$$\sigma_y(T,\dot{\varepsilon}) = \begin{cases} (-0.22T + 62)[\dot{\varepsilon}]^{(8.27\times 10^{-5}T + 0.0726)} & for \quad \dot{\varepsilon} \geq 5\times 10^{-4} \\ (0.723T + 105.22)[\dot{\varepsilon}]^{(1.6224\times 10^{-3}T + 0.1304)} & for \quad \dot{\varepsilon} < 5\times 10^{-4} \end{cases} \tag{14}$$

$$\sigma_{UTS}(T,\dot{\varepsilon}) = \begin{cases} (-0.25T + 76)[\dot{\varepsilon}]^{(2.06\times 10^{-4}T + 0.0825)} & for \quad \dot{\varepsilon} \geq 5\times 10^{-4} \\ (0.91T + 128.775)[\dot{\varepsilon}]^{(1.581\times 10^{-3}T + 0.1337)} & for \quad \dot{\varepsilon} < 5\times 10^{-4} \end{cases} \tag{15}$$

Therefore, equations (11), (14), and (15) are the final empirical formulae required to characterize Young's modulus, yield stress, and UTS of 63Sn/37Pb solder, respectively.

Multiple correction coefficient is used to measure the goodness of curve fitting in multiple linear regression. A multiple correction coefficient value of 1.0 represents a "perfect" fit. For the empirical models of Young's modulus, yield stress, and UTS, three values of 0.9678, 0.9755 and 0.981 are obtained, respectively. Therefore, the models do represent the data accurately. By plotting the estimated values against the experimental values, the visual pictures of the three models'

validity are shown in Fig. 11. From the picture, the data are arranged around a corresponding 45^{o} line. This line indicates where the estimated data and the experimental data are equal, i.e. a multiple correction coefficient value of 1.0.

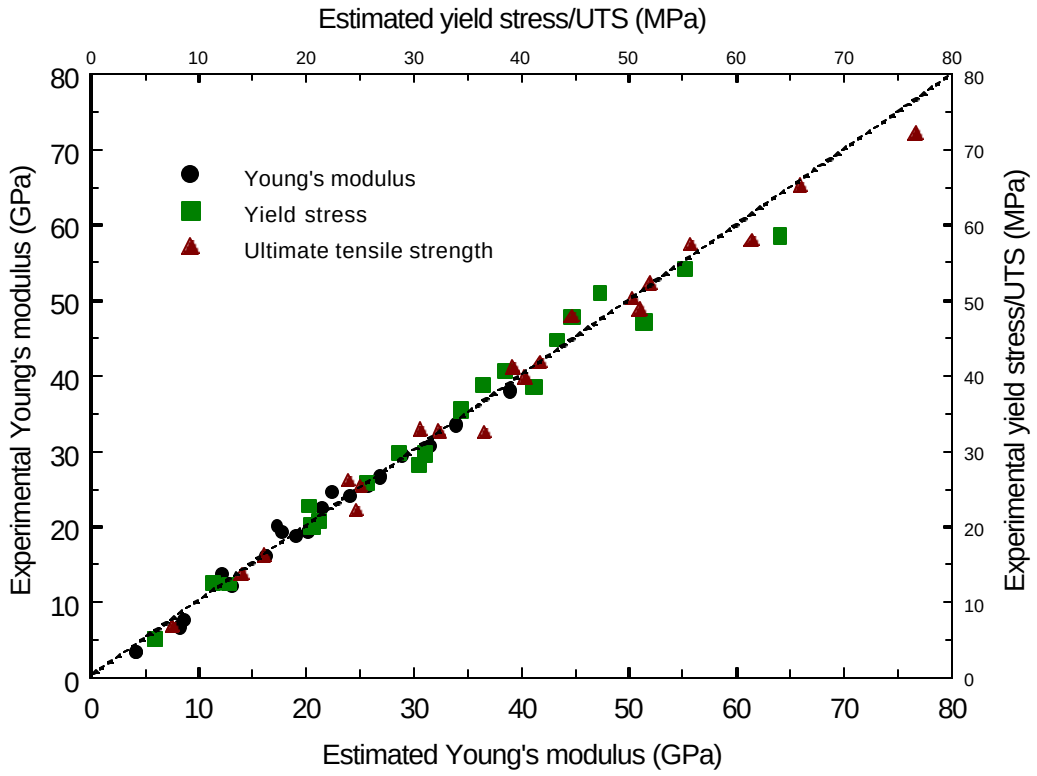

Fig. 11 Estimated mechanical properties versus experimental mechanical properties

5. Discussion

To verify their accuracy and validity further, the empirical formulae were used to predict and explain the wide range of different mechanical properties obtained by different researchers. Based on recent publications, some typical data provided by five researchers were chosen to study the differences in mechanical properties of 63Sn/37Pb. The details of testing conditions, temperature and strain rate dependent equations of the mechanical properties obtained by different

researchers are shown in Table 1. From Table 1, it is obvious that there are large variations in the mechanical properties reported because of different test conditions used.

Table 1 Details of results obtained by different researchers

Researchers	Test Method	Influence Factors		Results	
		Temperature	Strain Rate	Temperature Dependence	Strain Rate Dependence
Jones	acoustic pulse	$-200\ ^0$C ~ $150\ ^0$C	$3\times10^{-3}\ s^{-1}$	$E_2 = -0.0761T + 29.239$ *	not available
	uniaxial tension	$-200\ ^0$C ~ $150\ ^0$C	$3\times10^{-3}\ s^{-1}$	$E_1 = -0.00719T + 0.923$ * $\sigma_{0.2} = -0.26T + 45.332$ * $\sigma_{uts} = -0.35T + 50.737$ *	not available
Liu	uniaxial tension	$0\ ^0$C ~ $100\ ^0$C	$5.56\times10^{-3}\ s^{-1}$	$E = -0.11T + 26.3$ $\sigma_{0.2} = -0.154T + 43.4$ $\sigma_{uts} = -0.18T + 47.5$	not available
Lau	uniaxial tension	$-100\ ^0$C ~ $100\ ^0$C	$10^{-2}\ s^{-1}$	$E = -0.088T + 32$ $\sigma_{uts} = -0.2T + 53.263$	not available
			$5\times10^{-4}\ s^{-1}$	$\sigma_{0.2} = -0.246T + 38.43$	
Ninomiya	uniaxial tension	$0\ ^0$C $25\ ^0$C $100\ ^0$C	$3.3\times10^{-3}\ s^{-1}$ $3.3\times10^{-4}\ s^{-1}$ $3.3\times10^{-5}\ s^{-1}$	at strain rate $3.3\times10^{-3}\ s^{-1}$: $\sigma_{uts} = -0.25T + 52.4$ *	at temperature 25 ^{o}C : $\sigma_{0.2} = 67.2(\dot{\varepsilon})^{0.1154}$ *
Sandor	uniaxial tension	$23\ ^0$C ~ $100\ ^0$C	$2\times10^{-5}\ s^{-1}$	$E = -0.081T + 16.06$ *	not available

In this table, E, $\sigma_{0.2}$, σ_{uts}, and T represent Young's modulus (Gpa), yield stress (Mpa), ultimate tensile strength (Mpa), and temperature respectively. The equations remarked by the symbol " * " were obtained by fitting the author's raw data published in the corresponding references, the other equations were quoted directly from the references.

As an example, a comparison was made on the Young's modulus obtained by different researchers and our empirical model. As can be seen in Fig. 12, the wide range of Young's modulus properties depends heavily on the temperature and strain rate, but they can be predicted by the general formula (11). Similarly, the models of yield stress and UTS provided in the equations (14)

and (15) respectively can fit well the experimental yield stress and UTS's results obtained by different researchers also. Hence, it is concluded that the strain rate parameter is also very important in addition to the test temperature in order to obtain the approximate mechanical properties from 10^{-5} s^{-1} to 10^{-1} s^{-1} and – 40 ^{o}C to 125 ^{o}C.

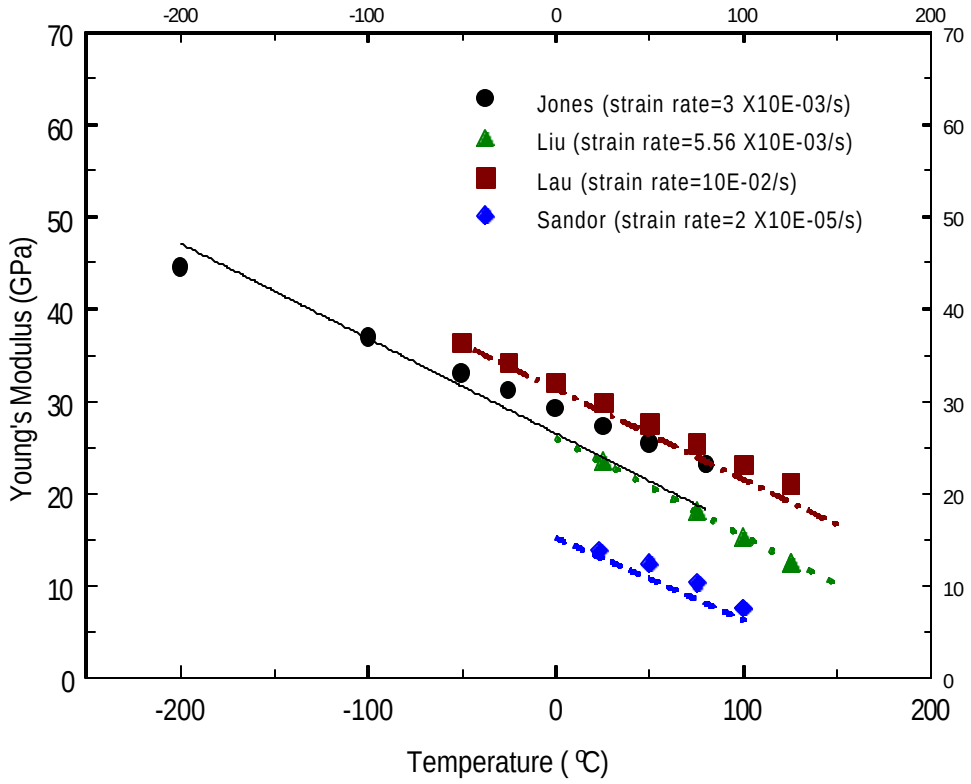

Fig. 12 Comparison on Young's modulus obtained by different researchers and our model: the symbols show the results obtained by different researchers, and the lines represent the results obtained by our empirical equation.

6. Conclusions

Based on our tests and analysis, the following conclusions have been reached:

1). The values of the mechanical properties of 63Sn/37Pb solder alloy depend strongly on test temperature and strain rate. The experimental results for Young's modulus E(T, $\dot{e}$), yield stress

$\sigma_y(T, \dot{e})$, and UTS $\sigma_{UTS}(T, \dot{e})$ have been curve-fitted to comprehensive constitutive equations given in equations (11), (14), and (15) respectively.

2). Using the temperature and strain rate dependent constitutive equations for $E(T, \dot{e})$, $\sigma_y(T, \dot{e})$, and $\sigma_{UTS}(T, \dot{e})$, the data on the mechanical properties provided by different reports for different test conditions of temperature and strain rate were represented satisfactorily. It is found that the apparently large differences in the data are mainly due to the different strain rates used in different laboratories.

3). At the temperature range of 0.4 T_m to 0.6 T_m, elongation shows an "unusual" relationship with temperature and strain rate, *i.e.*, elongation reaches a maximum value at the optimum test temperature of $-50\ ^oC$ and test strain rate of $2.78 \times 10^{-1}\ s^{-1}$. This quasi-superplasticity behavior is expected as the result of the interaction between work hardening and dynamic recovering.

Acknowledgments

The authors wish to thank the financial support provided by National Science & Technology Board, Singapore.

References

Furukawa, M., Ma, Y., Horita, Z., Nemoto, M., Valiev, R. Z., and Langdon, T. G., 1998, "Microstructural Characteristics and Superplastic Ductility in A Zn-22% Al Alloy with Submicrometer Grain Size," *Materials Science and Engineering*, A241, pp.122-128.

Han, B. Q., and Chan, K. C., 1997, "High-Strain-Rate Superplasticity of An AL2009-SIC_w Composite," *Journal of Materials Science Letters*, 16, pp.827-829.

JEDEC (Joint Electronic Device Engineering Council) Standard, 1989, "Temperature Cycling," *JESD22-A104-A*, Electronic Industries Association, USA.

JEDEC (Joint Electronic Device Engineering Council) Standard, 1995, "Thermal Shock," *JESD22-A106-A*, Electronic Industries Association, USA.

Jones, W. K., Liu,, Y. Q., Zampino, M. A., and Gonzalez, G. L., 1997, "The At-Temperature Mechanical Properties of Lead-Tin Based Alloys," *Advancing Microelectronics*, pp30-34.

Kilinski, T. J., Lesniak, J. R., and Sandor B. I., 1991, "Modern Approaches to Fatigue Life Prediction of SMT Solder Joints," *Solder Joint Reliability: Theory and Applications*, ed. J. Lau , pp384-390.

Kondo, T., Takigawa, Y., and Sakuma, T., 1997, "High-Temperature Tensile Ductility in TZP and TiO_2–Doped TZP," *Materials Science and Engineering*, A231, pp.163-169.

Lau, J., and Pao, Y. H., 1997, "Solder Joint Reliability of BGA, Flip Chip, CSP, and Fine Pitch SMT Assemblies," *New York: Van Nostrand Reinhold*, Chapter 4.

Li, M. Q., and Chen, Y., 1997, "Superplastic Deformation of SiC_p/2024 Al Composite Fabricated by Spray Atomization and Codeposition," *Journal of Materials Engineering and Performance*, Vol.6(5), pp.664-666.

Liu, S., and Qing, Z. F., 1997, "A Unified Viscoplastic Constitutive Model for Tin-Lead Solder Joints, " *Advances in Electronic Packaging*, ASME EEP-Vol.19-2, pp.1599-1604.

Ninomiya, R., and Miyake, K., 1997, "Microstructure and Mechanical Properties of New Lead-Free Solder," *Advances in Electronic Packaging*, pp.1329-1333.

Sandor, B. I., Ju, S. H., and Plesha, M. E., 1996, "Life Prediction of Solder Joints by Damage and Fracture Mechanics," ASME *Journal of Electronic Packaging*, Vol.118, pp193-200.

Skipor, A. F., S.V. Harren, and J. Botsis, 1996, "On the constitutive Response of 63/37 Sn/Pb Eutectic Solder," *ASME Journal of Engineering Materials and Technology*, Vol. 118, pp. 1-11.

Vaynman, S., and Fine, M. E., 1989, "Fatigue of Low-Tin Lead-Based and Tin-Lead Eutectic Solders," *Microelectronic Packaging Technology*, ed. W. T. Shieh, pp255-259.